JACS
JOURNAL OF THE AMERICAN CHEMICAL SOCIETY
Article
pubs.acs.org/JACS

A Noncrystallization Approach toward Uniform Thylakoids-like 2D "Nano-coins" and Their Grana-like 3D Suprastructures

Zhiwei Lin,[†] Jian Sun,[†] Yangbin Zhou,[†] Yu Wang,[†] Hui Xu,[†] Xing Yang,[†] Hao Su,[‡] Honggang Cui,[‡] Takuzo Aida,[§] Wei Zhang,*[,†] and Stephen Z. D. Cheng*[,†]

[†]Department of Polymer Science, College of Polymer Science and Polymer Engineering, The University of Akron, Akron, Ohio 44325, United States

[‡]Department of Chemical and Biomolecular Engineering, The Johns Hopkins University, 3400 N Charles Street, Baltimore, Maryland 21218, United States

[§]Department of Chemistry and Biotechnology, School of Engineering, The University of Tokyo, 7-3-1 Hongo, Bunkyo-ku, Tokyo 113-8656, Japan

Supporting Information

ABSTRACT: Two-dimensional (2D) circular shape nanostructures (e.g., "nano-coins") are ubiquitously present in thylakoids and grana within chloroplasts of plant cells in nature. The design and fabrication of 2D nano-coins with controlled sizes and thicknesses yet remain challenging tasks. Herein, we present a noncrystallization approach to achieve 2D nano-coins from assemblies of a set of zwitterionic giant surfactants. Distinguished from traditional crystallization approaches where the 2D nanostructures with specific crystallographic symmetries are fabricated, the noncrystallization assembly of giant surfactants results in 2D nano-coins that are derived from the separation of assembled 3D multiple lamellar cylindrical colloids with uniform diameters. The diameters and thicknesses of these nano-coins can be readily tailored by varying the molecular length of giant surfactants' tails. The formation of 2D nano-coins or 3D cylindrical colloid suprastructures is controlled by tuning the pH value of added selective solvents. This new strategy opens a door for controlling the shape, size, and size distribution of assembled nanostructures with different hierarchies.

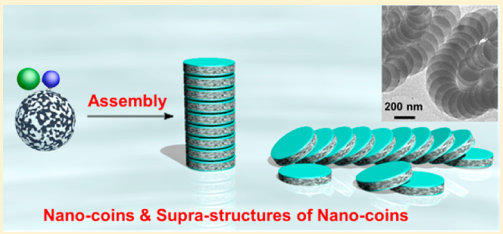

INTRODUCTION

Today hierarchically assembled two-dimensional (2D) nanostructures have been extensively studied due to their unique dimensional-dependent properties.[1] Most of current techniques for preparing 2D assembled nanostructures involve crystallization processes at certain stages, such as 2D hierarchical nanosheets formed by crystallization-driven assembly of homopolymers and block copolymers,[2] 2D nanocrystals of molecular Janus particles[3] or peptoid polymers,[4] and the generation of dynamic 2D protein crystals from rotational symmetric proteins.[5] The overall shapes of these 2D nanostructures are thus dominated by crystallization to form flat Wulff shapes which possess a C_2-, C_3-, C_4-, or C_6-rotational symmetry as a result of the crystal unit cell symmetry (Figure 1a),[2a,5,6] and the size of resultant 2D crystals is rarely controlled, if possible, in a self-seeding process.[7] Despite these successes, methods to prepare circular-shaped 2D nanostructures are still largely unexplored, since this type of structures does not contain crystallographically defined lateral surfaces and, thus, requires a noncrystallization approach. In certain assembling conditions, spherical micelles could be deformed and exhibit disk-like quasi 2D nanostructure;[8] however, their size, size distribution, and thickness control remain grand challenges. We are devoted to the preparation of precisely controlled circular-shaped 2D nanostructures (like "nano-coins"), which ubiquitously present and play critical roles in nature, such as in chloroplasts of plant cells.[9] One chloroplast contains many cylindrical structures (called grana), and each cylinder is formed via stacking of 2D nano-coin thylakoids (Figure 1b), acting to trap the energy from sunlight.[10] These unique nano-coin thylakoids and their stacking grana ensure an extremely large area-to-volume ratio for photosynthetic reaction, a high stability, and flexibility in response to dynamically changed environmental conditions.[11]

In this article, we report a simple approach to achieve well-defined 2D nano-coins via designed zwitterionic giant surfactants. Inspired by 2D crystals based on molecular Janus nanoparticles reported by our group,[3] this series of zwitterionic giant surfactants is composed of ionic heads having both positively and negatively charged fullerenes (C_{60}) and a hydrophobic nonpolar polystyrene (PS) tail (abbreviated as $NC_{60}^{+}-AC_{60}^{-}-PS_n$, Figure 1c), which yet feature noncrystallinity. The molecular design of these zwitterionic giant surfactants captures the essential structural feature of small-molecular zwitterionic surfactants,[12] but with amplified molecular sizes.[13] In the meantime, pH-responsive groups on the heads of giant surfactants afford the response capability of external conditions. After self-assembling in solution, highly uniform

Received: February 6, 2017
Published: April 7, 2017

DOI: 10.1021/jacs.7b01275
J. Am. Chem. Soc. 2017, 139, 5883−5889

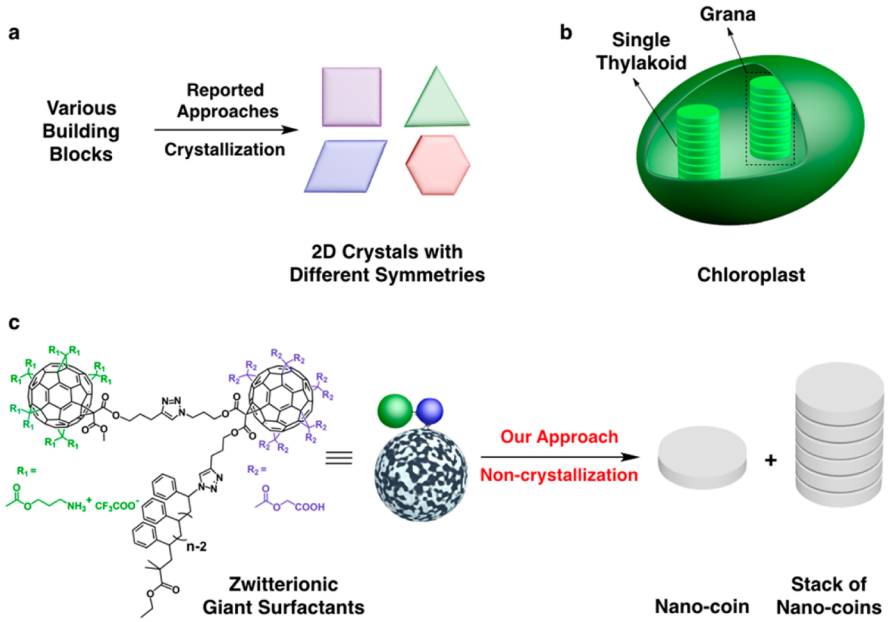

Figure 1. Traditional and our approaches for fabricating 2D nanostructures in solution. (a) General crystallization-based approaches for 2D nanostructures with regular shapes and different rotational symmetry. (b) Schematic representation of a chloroplast containing 2D nano-coin thylakoids and the cylindrically stacked thylakoids (grana). (c) Chemical structure of a zwitterionic giant surfactant, NC_{60}^{+}–AC_{60}^{-}–PS_n. The cartoon is a simplified molecular model of NC_{60}^{+}–AC_{60}^{-}–PS_n, in which green and blue spheres represent amino- and carboxyl-functionalized C_{60}, tethered with a PS random coil. Round-shape 2D nano-coins and their 3D stacking structures are formed through the current noncrystallization approach.

2D circular shaped nano-coins with controlled lateral sizes and thicknesses are achieved. These 2D nano-coins are able to further stack together to form cylindrical 3D suprastructures at certain conditions. The hierarchically assembled structures resemble the features of thylakoids and grana structures in chloroplasts.

RESULTS AND DISCUSSION

Molecular Design. A series of zwitterionic giant surfactants with different molecular tail lengths of PS were synthesized by a sequential copper-catalyzed azide–alkyne "click" reaction [see Supporting Information (SI), Scheme S1]. Their well-defined chemical structures and high purities were fully characterized (Figures S1–S6). The precursor of NC_{60}^{+}–AC_{60}^{-}–PS_n (compound 7) bears a *tert*-butoxy carbamate (Boc)-protected C_{60} and a *tert*-butyl-protected C_{60}. After treating with excessive trifluoroacetic acid (CF_3COOH), both Boc and *tert*-butyl groups were readily hydrolyzed, affording positively charged amino groups with CF_3COO^{-} groups as counterions[14] and neutral carboxylic groups.[15] Since carboxylic acid groups can be partially ionized in solution,[13b] the zwitterionic attributes of giant surfactants are endowed as dissolving in polar solvents where the degree of ionization of carboxylic acid groups can be tuned by the concentration of free hydrogen ions in solution. Such molecular design renders the giant surfactants versatile assembling structures controlled by the pH value of solution.

Formation of Thylakoid-like 2D Nano-coins. Two parameters were focused on in our investigation of solution-assembly behaviors of this series of zwitterionic giant surfactants: an internal structure parameter of the length of PS tail in these surfactants, and an external parameter of the pH value of added aqueous selective solvents. The first experiment was performed by adding HCl aqueous solution (pH = 5, 1.5 mL) into THF (comment solvent) solution of NC_{60}^{+}–AC_{60}^{-}–PS_{86} (c = 1 mg/mL, 1 mL) at 20 °C (see details in SI). After stirring the mixture at 20 °C for 2 h, air-dried samples were examined by transmission electron microscope (TEM). Uniform individual 2D nano-coins with a diameter around 250 nm were observed (Figure 2a). Based on the results obtained from atom force microscopy (AFM), the thicknesses of these nano-coins were measured to be 15.3 ± 0.2 nm (Figure 2b and c).

We have confirmed that individual nano-coins can also be observed by adding HCl aqueous solution with their pH values ranging between 3 and 5 into NC_{60}^{+}–AC_{60}^{-}–PS_{86}/THF solution (Figures S7 and S8). We also noted that the 2D nano-coins structures were stable over a period of three months. When the length of PS tail was decreased to 62 repeating units, an individual nano-coin with a diameter of 250 nm was also observed (Figure 2d), while the thickness of the resulting individual nano-coin is decreased to 12.7 ± 0.3 nm, as measured by AFM (Figure 2e and f). When the length of PS tail was increased to 120 repeating units, nano-coins with a thickness of 17.5 ± 0.5 nm were found (Figure S9) but, however, have a relatively wide distribution in their diameters (Figure S10). If considering that the diameter of ionized C_{60} is around 2 nm[15b,16] and the radii of gyration (R_g) of PS are 2.18 and 2.57 nm for PS_{62} and PS_{86} (see SI for calculations), respectively, the resulting individual thicknesses of nano-coins can be qualitatively judged that they consist of a single layer of zwitterionic giant surfactant heads at both of the top and bottom, and two layers of the PS tails are sandwiched in between as illustrated in Figure 2g and h. Furthermore, wide-angle X-ray diffraction (WAXS) and electronic diffraction (ED) results of 2D nano-coins confirm their noncrystalline feature within the nano-coins (Figure S11).

To understand the formation pathway and mechanism of the nano-coins, dynamic light scattering (DLS) experiments were carried out to investigate their solution assembly behaviors. Typical CONTIN analyses of DLS measurements for these three samples indicate that the formation of assembled structures have an average hydrodynamic radius (R_h) of 350 nm with minor angular dependence (Figure S12a for NC_{60}^{+}–AC_{60}^{-}–PS_{62} as an

DOI: 10.1021/jacs.7b01275
J. Am. Chem. Soc. 2017, 139, 5883–5889

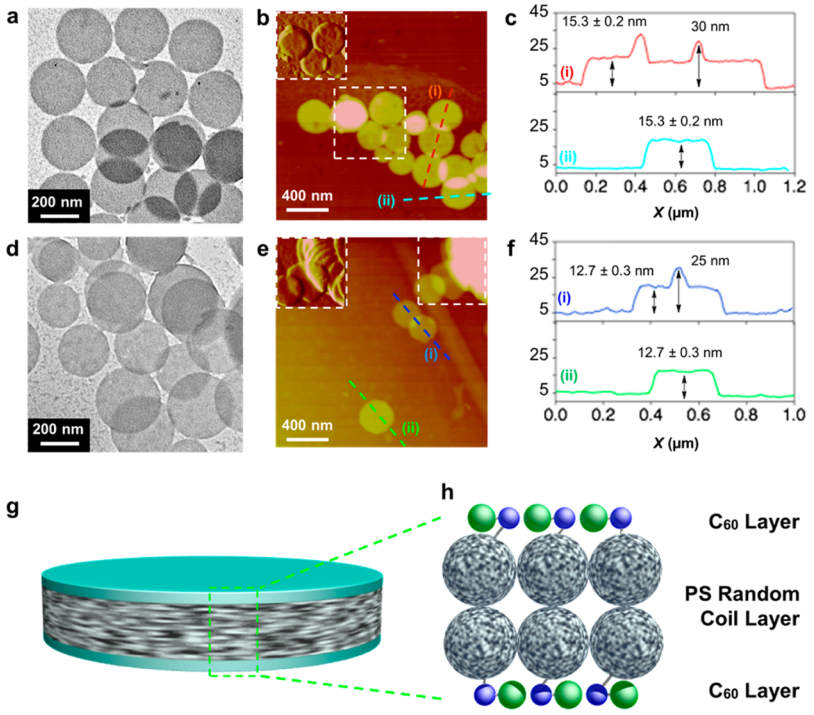

Figure 2. Morphological characterization of 2D nano-coins. (a) Bright-field TEM images of NC_{60}^{+}–AC_{60}^{-}–PS_{86}, prepared by adding aqueous HCl solution (pH = 5) into giant surfactants in THF solution. (b) AFM image of NC_{60}^{+}–AC_{60}^{-}–PS_{86} in the height mode. The upper-left inset is the amplitude image in selective area. (c) The height profiles of 2D nano-coins in panel b. (d) Bright-field TEM images of NC_{60}^{+}–AC_{60}^{-}–PS_{62}, prepared by adding aqueous HCl solution (pH = 5) into giant surfactants in THF solution. (e) AFM image of NC_{60}^{+}–AC_{60}^{-}–PS_{62} in the height mode. The upper-left inset is the amplitude image in upper-right selective area. (f) Height profiles of 2D nano-coins in panel e. (g) Schematic representation and (h) molecular packing of a 2D nano-coin formed by an assembly of zwitteronic giant surfactants.

example), suggesting the presence of close to isotropic aggregates in the solution. Their R_h values are much larger than the size of individual 2D nano-coin, further revealing that the stacked rather than well-dispersed nano-coins present in the solution (Figure S12a for NC_{60}^{+}–AC_{60}^{-}–PS_{62} as an example). The detailed internal structure of these stacking of 2D nano-coin structures for NC_{60}^{+}–AC_{60}^{-}–PS_{62} is revealed by cryo-TEM imaging without staining. As shown in Figure 3a, cylinder-like colloids having multiple layers are observed. The building blocks are layered structures with identical thickness and diameter (lateral size). Since the electron density of C_{60} is higher than that of PS, the dark layers are attributed to the aggregation of the zwitterionic C_{60} heads with a layer thickness of around 6.5 ± 0.3 nm (Figure 3b). Note that this thickness is about 2.5 nm larger than the estimated double layer thickness of ionized C_{60} heads (4 nm). The combination of the DLS and cryo-TEM results verifies the formation of multiple layered cylindrical colloids rather than individual nano-coins in solution. Fourier transform infrared (FTIR) results on the freeze-dried powder samples of NC_{60}^{+}–AC_{60}^{-}–PS_{62} reveal around 28% of carboxylic groups are deprotonated (Figure S13), indicating that surfaces of the nano-coins are overall positively charged, which is further confirmed by zeta potential result of sample (for NC_{60}^{+}–AC_{60}^{-}–PS_{62}, +65.3 mV) in solution. The static charge repulsion between the C_{60} layers may lead to a relatively loose layer packing. All of these experimental results suggest that the nano-coins are derived from the separation of cylindrical colloids containing multiple layered structures, reminiscent of the falling of a cylindrical column of well-stacking coins. A direct evidence of this assessment is that we can occasionally observe in real space the existence of partially fallen nano-coins with one stacked on another under cryo-TEM for steered NC_{60}^{+}–AC_{60}^{-}–PS_{62} solution (Figure 3c). Furthermore, we can also observe under bright-field TEM for the same samples; in many cases, uniform nano-coins are lying down and partially stacked one by one, similar to the case after "circular Domino in falling" as shown in Figure 2d. The similar observation for NC_{60}^{+}–AC_{60}^{-}–PS_{86} is also clearly presented in Figure 2e. The separation of individual "coins" is attributed to the charge repulsion between layer surfaces of ionized C_{60}, yet further revealing that the two zwitterionic C_{60} heads in one giant surfactant are located in the same C_{60} head layer of the "coin" due to the PS tail chemical linking location to the C_{60} head (Figure 2h). Otherwise, if there is a connection between two C_{60} head layers, this separation of the individual coin could not be possible. The formation pathway is thus proposed in Figure 3f. The nano-coins are generated via nanophase separation between C_{60} and PS tails inside the cylindrical colloids and thus possess identical diameters. Due to the loose packing between two C_{60} layers, they will fall down and form a "circular Domino in falling" after solvent evaporating as observed in Figure 3d and e.

The Formation of Grana-like 3D Suprastructures of Stacked 2D Nano-coins. The uniform 2D nano-coins and their cylindrical colloid suprastructures in solution (Figure 3a–e) resemble hierarchical assembly behaviors of thylakoids and grana that are observed within chloroplasts. The cylindrical colloids of stacked 2D nano-coins are formed in solution and falling into 2D nano-coins during the removal of solvents. While the repulsive charge interaction tends to separate the nano-coins, the hydrophobic effect and van der Waals interactions counter that tendency. We envision that, by lowering the positive charge repulsion between the surface layers of nano-coins, we may be

DOI: 10.1021/jacs.7b01275
J. Am. Chem. Soc. 2017, 139, 5883–5889

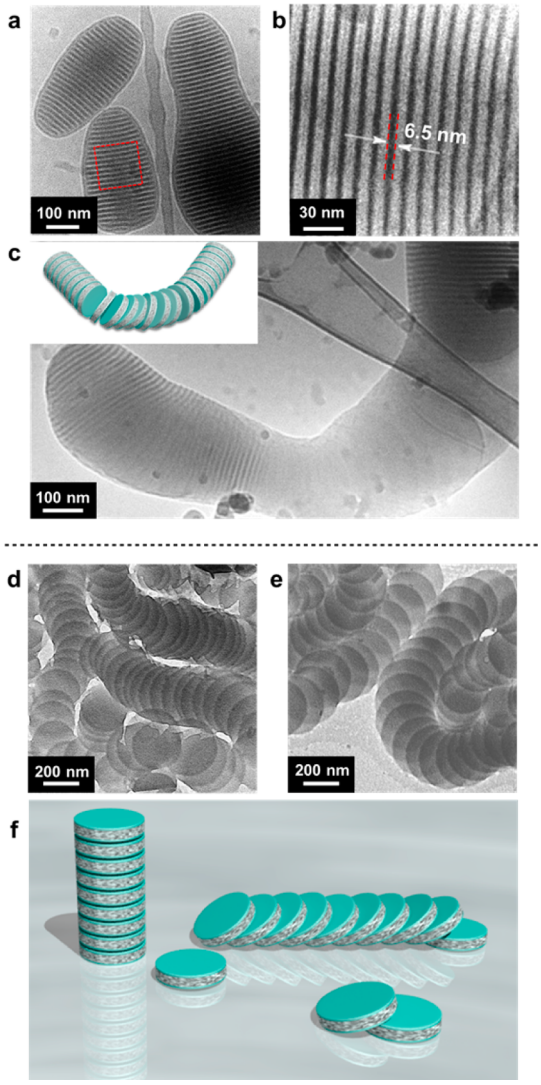

Figure 3. Formation pathway and mechanism of the 2D nano-coins. (a) Cryo-TEM image of NC_{60}^{+}–AC_{60}^{-}–PS_{62} in THF/aqueous HCl (pH = 5) solution, where the nano-coins are stacking together. (b) High-magnification cryo-TEM image for the selective area shown in panel a. (c) Cryo-TEM image of steered NC_{60}^{+}–AC_{60}^{-}–PS_{62} solution, where the partially separated and stacked nano-coins are presented. The inset is the cartoon illustrating the structures in the cryo-TEM image. Bright-field TEM images of (d) NC_{60}^{+}–AC_{60}^{-}–PS_{62} and (e) NC_{60}^{+}–AC_{60}^{-}–PS_{86} in THF/aqueous HCl (pH = 5) solution, where the 2D nano-coins are stacking one by one, resembling a collapse of a stack of "coins". (f) Schematic illustration of the discrete nano-coins when samples are dried out.

able to fabricate 3D cylindrical colloids of stacked nano-coins. Given by the fact that the degree of ionization of −COOH is inversely proportional to the concentration of free hydrogen ions, we carried out the assembly process by adding neutral water (pH = 7, 1.5 mL) into THF solution of giant surfactants (c = 1 mg/mL, 1 mL) at 20 °C, in which FTIR results indicate that the degree of ionization of −COOH is around 38% (Figure S13). Cylindrical colloids are formed with an average diameter of around 250 nm for NC_{60}^{+}–AC_{60}^{-}–PS_{62} under this condition (Figure 4a), in good agreement with the diameter of individual nano-coins. Scanning electron microscopy (SEM) image (Figure 4a, inset) allows for the visualization of 3D cylindrical colloids. Within these cylindrical colloids, well-stacked layers with alternatively dark (C_{60}) and gray (PS) layers are presented. It should be pointed out that, once the cylindrical colloids are formed in this condition, further adding lower pH values of HCl aqueous solution will not alter the final colloid morphology. No separation of nano-coins was observed after the samples were dried and prepared for TEM observations.

With increasing the length of the PS-tails to n = 86, the cylindrical colloids with stacked layers also possess a diameter of around 250 nm as identified by TEM (Figure 4b) and SEM (Figure 4b, inset) observations. In theory,[17] when the size of PS tail is much bigger than that of the zwitterionic C_{60} heads, the assembly behavior of this molecule will be dominated by PS tails. In this case, the surface free energy of colloids dominates the assembling process, and the overall shape becomes spherical.[18] Indeed we found that, when the PS tail with 120 repeating units was used, spherical colloids with partial layer stacks near the center of the colloids were observed, yet they possess a diameter of 220 nm (Figure 4c). It can be expected that if the "circular Domino in falling" collapsing of the cylinder colloids takes place as the overall positive surface charge of the C_{60} layer increases (decreasing the pH value of added HCl aqueous solution), uniform 2D nano-coins would be produced. If the colloid shape deviates from cylindrical (such as becoming spherical), the 2D nano-coins with a broad distribution of their lateral sizes-(diameters) can be expected.

Figure 4d–f shows bright-field TEM images for three cylindrical colloids with a high-magnification in the selective area of Figure 4a–c. Their corresponding fast Fourier transform (FFT) patterns are also inserted in these figures. When we compare the nano-coins stacked structures formed in these three samples, it is found that the thicknesses of the darker C_{60} layers keep constant at around 4.0 nm, consistent with a double size of diameters of the close-packed ionized C_{60} heads. Those of greyer PS layers increase from 8.6 nm, to 11.0 to 12.5 nm, with an increasing of PS tail length from n = 62, to n = 86, and further to n = 120, respectively.

The colloid growth process can be monitored by TEM at different water contents (Figure S14). As neutral water was added into the NC_{60}^{+}–AC_{60}^{-}–PS_n/THF solution, hydrophobic PS tails tend to aggregate and stimulate nanophase separation between ionized C_{60} heads and nonpolar PS tails due to the incompatibility between two components.[18,19] The growth direction along the layer normal is governed by the aggregation of the PS tails and zwitterionic C_{60} heads which have been neutralized by the counterions in solution. The lateral growth perpendicular to the layer normal is attributed to accumulative addition of the zwitterionic giant surfactants into assemblies. When the PS tails are overcrowded, they could be squeezed out from the PS layers and eventually cover the edges of the C_{60} head ionic layers to prevent their further lateral growth. The overall shape of the colloids is governed by minimizing overall surface free energy.[17]

The squeezed PS tails can be described by the concept of reduced tethering densities ($\tilde{\sigma}$) of PS tethered on a flat surface.[20] It is defined by

$$\tilde{\sigma} = \sigma\pi R_g^{\,2} \qquad (1)$$

where R_g is the radius of gyration of PS chain, and σ is the tethering density, defined as the reciprocal average covering area of each chain. It has been experimentally proved that the tethered chains start to be squeezed by their neighboring chains at a critical $\tilde{\sigma}^* \sim 3.7$.[20,21] The $\tilde{\sigma}$ values for our three samples have been calculated to be 4.1, 5.8, and 8.1 (see calculations in SI),

DOI: 10.1021/jacs.7b01275
J. Am. Chem. Soc. 2017, 139, 5883–5889

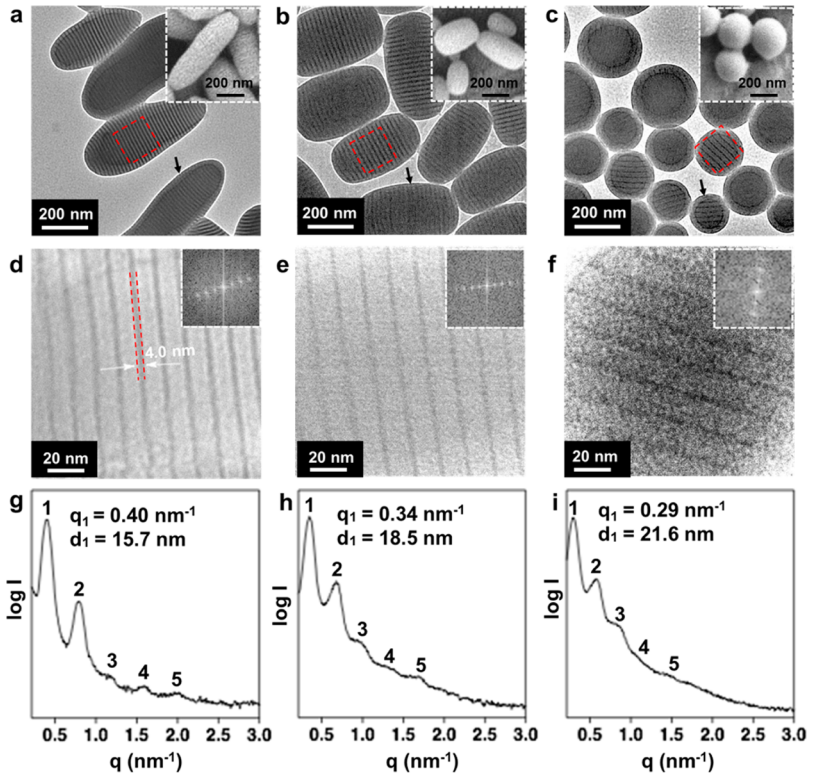

Figure 4. Formation of cylindrical colloids of stacked 2D nano-coins and the comparison of their lamellae thicknesses with those formed in bulk states. Bright-field TEM images of (a) NC_{60}^{+}–AC_{60}^{-}–PS_{62}, (b) NC_{60}^{+}–AC_{60}^{-}–PS_{86}, and (c) NC_{60}^{+}–AC_{60}^{-}–PS_{120}, prepared by adding neutral water (pH = 7) into their THF solutions, respectively. Insets are the corresponding SEM images. Panels d, e, and f are high-magnification TEM images of the selective area in panels a, b, and c. The insets are the FFT patterns of the TEM images. SAXS patterns of (g) NC_{60}–AC_{60}–PS_{62}, (h) NC_{60}–AC_{60}–PS_{86} and (i) NC_{60}–AC_{60}–PS_{120} in bulk states, prepared by thermal annealing at 130 °C for 12 h.

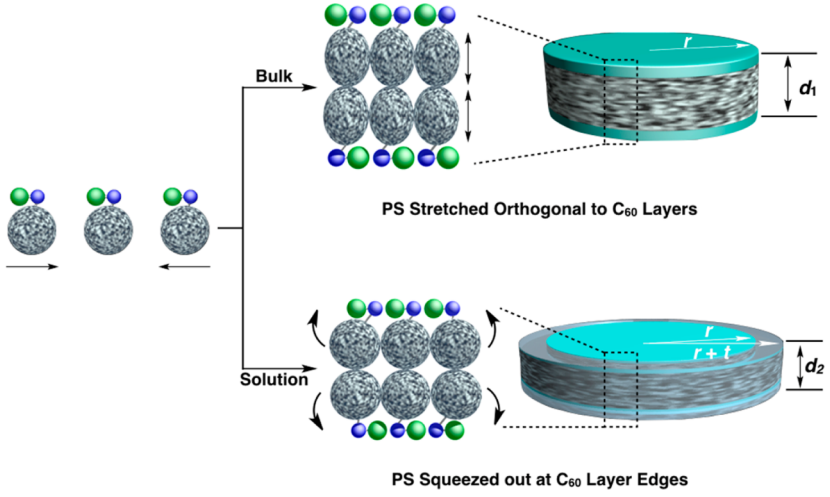

Figure 5. Stretching and squeezing of PS in the bulk and solution state. In bulk state, PS chains are stretched orthogonal to the C_{60} layer, where a radius (r) is assigned and the thickness (d_1) can be obtained from SAXS results. In solution state (cylindrical colloids), the PS chains are squeezed out at C_{60} layer edges. The thickness (d_2) can be obtained from TEM images in Figure 4. After squeezing, the radius of column is $r + t$, where t is the PS layer thickness surrounding the column and can be measured from TEM image in Figure S15.

respectively, indicating that the PS tails are overcrowded. If the layer lateral dimension is infinitely large, the squeezed PS tails must be stretched orthogonal to the layer (Figure 5, in bulk state), leading to an increase of the layer spacing. However, if the lateral layer dimension starts growing at a limited size such as in the present case, the PS tails could be squeezed out at the edges of the layers (Figure 5, in solution state). The PS tail coverage on the periphery of C_{60} ionic layer edges can be directly observed in bright-field TEM images (arrows in Figure 4). Specifically, a more clear observation is available from high magnification TEM images (Figure S15), where a PS layer with thickness of ca. 12.5 and 11.9 nm is covered in the front of the C_{60} ionic layers in the case of NC_{60}^{+}–AC_{60}^{-}–PS_{62} and NC_{60}^{+}–AC_{60}^{-}–PS_{86}, respectively.

To quantitatively understand the overcrowding and squeezing out of the PS tails, we compare the d-spacing of the layers in the

DOI: 10.1021/jacs.7b01275
J. Am. Chem. Soc. 2017, 139, 5883–5889

Table 1. Molecular Information for Three Zwitterionic Giant Surfactants

sample	N^a	$R_g{}^b$ (nm)	$\tilde{\sigma}^c$	$d_1{}^d$ (nm)	$d_2{}^e$ (nm)	$L_1{}^f$ (nm)	$L_2{}^g$ (nm)	$S_1{}^h$	$S_2{}^i$
NC_{60}–AC_{60}–PS_{62}	62	2.18	4.1	15.7	12.6	5.9	4.3	1.35	0.99
NC_{60}–AC_{60}–PS_{86}	86	2.57	5.8	18.5	15.0	7.3	5.5	1.41	1.07
NC_{60}–AC_{60}–PS_{120}	120	3.04	8.1	21.6	16.5	8.8	6.3	1.45	1.04

[a]The number of repeating units in PS. [b]Radius of gyration of PS. [c]Reduced tethering density of PS. [d]Periodic lamellar *d*-spacings in bulk. [e]Periodic lamellar *d*-spacings in cylindrical colloids. [f]Half layer thicknesses of the PS domain in bulk. [g]Half layer thicknesses of the PS domain in cylindrical colloids. PS layer thicknesses in bulk state can be obtained by deducting C_{60} layer thickness from d_1. [h]Stretching ratios of PS tails in bulk. [i]Stretching ratios of PS tails in cylindrical colloids.

cylindrical colloids with those formed in the solid state of these zwitterionic giant surfactants. After thermally annealed at 130 °C for 12 h in the bulk, well-ordered, layered structures were observed for all three samples of NC_{60}–AC_{60}–PS_{62}, NC_{60}–AC_{60}–PS_{86}, and NC_{60}–AC_{60}–PS_{120}, evidenced by the *q*-ratios of 1:2:3:4:5 in the small-angle X-ray scattering (SAXS) patterns (Figure 4g–i), indicating that the multiple layered structures are formed by the nanophase separation of the C_{60} ionized heads and PS tails. Since the PS tails in the bulk cannot be squeezed out at the layer edges, the *d*-spacings of the layers formed in the bulk must be larger than those in cylindrical colloids. This is indeed the case as experimentally observed: 15.7 nm vs 12.6 nm for NC_{60}–AC_{60}–PS_{62}, 18.5 nm vs 15.0 nm for NC_{60}–AC_{60}–PS_{86}, and 21.6 nm vs 16.5 nm for NC_{60}–AC_{60}–PS_{120}, respectively, as summarized in Table 1. Therefore, the PS tails in the bulk state are expected to be more stretched than those in cylindrical colloids. The stretching ratio (S) of PS tails in the cylindrical colloids and the bulk state can be quantitatively characterized by[22]

$$S = L/2R_g \tag{2}$$

where L is the half layer thickness of PS domain. The S values are close to unity in cylindrical colloids (S_2 values in Table 1) for these three samples, while they range from 1.35 to 1.45 in the bulk state (S_1 values in Table 1). These results indicate that the PS tails are stretched in the bulk state but not so in the cylindrical colloids. To minimize free energy, the PS tails in the cylindrical colloids tend to be released and squeezed on to free layer edges. This type of tendency is accumulative.

In view of a constant PS density in both cases, the volume of PS tails (V_a) that are squeezed out at the layer edges can be calculated by,

$$V_a = \pi r^2(d_1 - d_2) \tag{3}$$

where r is a radius of an assumed column in the bulk and d_1 and d_2 are periodic lamellar *d*-spacing in the bulk and cylindrical colloids, where they include one PS domain and two layers of C_{60} (Figure 5). Note that the C_{60} layer thickness in the bulk state is also ca. 4.0 nm (Figure S16), identical to that in the cylindrical colloids. The volume of PS layer covered on the lateral growth surface of the C_{60} ionic layers can be calculated by

$$V_b = [\pi(r + t)^2 - \pi r^2] \times d_2 \tag{4}$$

where t is the thickness of PS layer along the radial direction covering on the lateral growth surface of the C_{60} ionic layers (Figure 5).

When one has $V_a = V_b$, indicating the lateral growth surface of C_{60} ionic layers are completely covered by the PS tails, a radius of cylindrical colloids ($r + t$) can be calculated to be 120.0 nm for $NC_{60}{}^+$–$AC_{60}{}^-$–PS_{62} and 119.5 nm for $NC_{60}{}^+$–$AC_{60}{}^-$–PS_{86}, or their diameters are 240.0 and 239.0 nm, respectively (see calculation in the SI). They are close to our experimental observation of 250 nm as shown in Figure 4a–b.

Assembling Behaviors under Other pH Values. Using HCl aqueous solution (pH ≤ 2) as selective solvent, regular micellar behaviors of giant surfactants in solution were exhibited. For example, by adding HCl aqueous solution (pH = 1)[23] into the THF solution of the giant surfactants (c = 1 mg/mL) at 20 °C, the ionization of carboxylic groups in the head are completely suppressed (Figure S13), and only positively charged C_{60} heads are functioning with hydrophobic PS tails in the assembly process. We thus observe the normal micellar formations, and they change from spheres, to cylinders, further to vesicles with increasing the length of PS tails from $NC_{60}{}^+$–AC_{60}–PS_{62}, to $NC_{60}{}^+$–AC_{60}–PS_{86} and further to $NC_{60}{}^+$–AC_{60}–PS_{120} (Figure S17), consistent with the solution assembly behaviors of our previously reported giant surfactants.[13b,15b]

CONCLUSIONS

In summary, we report a noncrystallization self-assembly approach to achieve unique round-shape 2D nano-coins with controlled sizes and thicknesses from zwitterionic giant surfactants. Differentiating from the crystallization-driven approaches where delicate control of crystallization conditions is essential and each individual single crystal 2D nanostructure grows independently, the self-assembly process of zwitterionic giant surfactant is readily directed by the strong nanophase separation between ionized C_{60} heads and nonpolar PS tails to generate the 3D cylindrical colloids with internal disk-stacked structures. The noncrystallization anisotropic growth lead to the round shape of cylindrical colloids, whose sizes is controlled by the full coverage of overcrowding and squeezing out PS layer on the periphery. These 3D cylindrical colloids ensure the uniform diameter of nano-coins. More importantly, the as-formed 3D cylindrical colloids can either be stabilized as suprastructures with controllable morphologies, or separated into 2D nano-coins by simply tuning pH value of the added selective solvents. This hierarchal assembly pathway resembles 2D nano-coin thylakoids stacking together to form 3D cylindrical grana in chloroplasts. This strategy is easily practicable and expected to be readily applicable to many other noncrystalline polymer systems. In addition to using templates and controlling kinetics during assembling process (e.g., living self-assembling process), this work affords us a new methodology to control the shape, size, and size distribution of assemblies in solution.

ASSOCIATED CONTENT

Supporting Information

The Supporting Information is available free of charge on the ACS Publications website at DOI: 10.1021/jacs.7b01275.

Experimental details, additional results and discussion (PDF)

DOI: 10.1021/jacs.7b01275
J. Am. Chem. Soc. 2017, 139, 5883–5889

AUTHOR INFORMATION

Corresponding Authors

*wzhang@uakron.edu
*scheng@uakron.edu

ORCID

Hui Xu: 0000-0002-6049-0123
Honggang Cui: 0000-0002-4684-2655
Takuzo Aida: 0000-0002-0002-8017
Stephen Z. D. Cheng: 0000-0003-1448-0546

Notes

The authors declare no competing financial interest.

ACKNOWLEDGMENTS

We thank Mr. Jiancheng Luo and Prof. Tianbo Liu for the help with light scattering experiment and analyses and Ms. Jie Yu and Prof. Steven Chuang for offering kind help in FTIR tests and analyses. This work is supported by National Science Foundation (NSF) Grant DMR-1408872.

REFERENCES

(1) (a) Nasilowski, M.; Mahler, B.; Lhuillier, E.; Ithurria, S.; Dubertret, B. *Chem. Rev.* **2016**, *116*, 10934−10982. (b) Zhuang, X.; Mai, Y.; Wu, D.; Zhang, F.; Feng, X. *Adv. Mater.* **2015**, *27*, 403−427. (c) Boott, C. E.; Nazemi, A.; Manners, I. *Angew. Chem., Int. Ed.* **2015**, *54*, 13876−13894. (d) Kissel, P.; Murray, D. J.; Wulftange, W. J.; Catalano, V. J.; King, B. T. *Nat. Chem.* **2014**, *6*, 774−778. (e) Zhu, J.; Zhang, S.; Zhang, K.; Wang, X.; Mays, J. W.; Wooley, K. L.; Pochan, D. J. *Nat. Commun.* **2013**, *4*, 2297. (f) Ni, B.; Huang, M.; Chen, Z.; Chen, Y.; Hsu, C.-H.; Li, Y.; Pochan, D.; Zhang, W.-B.; Cheng, S. Z. D.; Dong, X.-H. *J. Am. Chem. Soc.* **2015**, *137*, 1392−1395. (g) Robertson, E. J.; Olivier, G. K.; Qian, M.; Proulx, C.; Zuckermann, R. N.; Richmond, G. L. *Proc. Natl. Acad. Sci. U. S. A.* **2014**, *111*, 13284−13289. (h) Winfree, E.; Liu, F.; Wenzler, L. A.; Seeman, N. C. *Nature* **1998**, *394*, 539−544. (i) Colson, J. W.; Woll, A. R.; Mukherjee, A.; Levendorf, M. P.; Spitler, E. L.; Shields, V. B.; Spencer, M. G.; Park, J.; Dichtel, W. R. *Science* **2011**, *332*, 228−231. (j) Kory, M. J.; Wörle, M.; Weber, T.; Payamyar, P.; van de Poll, S. W.; Dshemuchadse, J.; Trapp, N.; Schlüter, A. D. *Nat. Chem.* **2014**, *6*, 779−784. (k) Kissel, P.; Erni, R.; Schweizer, W. B.; Rossell, M. D.; King, B. T.; Bauer, T.; Götzinger, S.; Schlüter, A. D.; Sakamoto, J. *Nat. Chem.* **2012**, *4*, 287−291. (l) Liu, W.; Halverson, J.; Tian, Y.; Tkachenko, A. V.; Gang, O. *Nat. Chem.* **2016**, *8*, 867−873. (m) Lee, M.; Park, M.-H.; Oh, N.-K.; Zin, W.-C.; Jung, H.-L.; Yoon, D. K. *Angew. Chem., Int. Ed.* **2004**, *43*, 6465−6468. (n) Wu, D.; Liu, R.; Pisula, W.; Feng, X.; Müllen, K. *Angew. Chem., Int. Ed.* **2011**, *50*, 2791−2794.

(2) (a) He, X.; Hsiao, M.-S.; Boott, C. E.; Harniman, R. L.; Nazemi, A.; Li, X.; Winnik, M. A.; Manners, I. *Nat. Mater.* **2017**, *16*, 481−488. (b) Hudson, Z. M.; Boott, C. E.; Robinson, M. E.; Rupar, P. A.; Winnik, M. A.; Manners, I. *Nat. Chem.* **2014**, *6*, 893−898.

(3) (a) Liu, H.; Hsu, C.-H.; Lin, Z.; Shan, W.; Wang, J.; Jiang, J.; Huang, M.; Lotz, B.; Yu, X.; Zhang, W.-B.; Yue, K.; Cheng, S. Z. D. *J. Am. Chem. Soc.* **2014**, *136*, 10691−10699. (b) Liu, H.; Luo, J.; Shan, W.; Guo, D.; Wang, J.; Hsu, C.-H.; Huang, M.; Zhang, W.; Lotz, B.; Zhang, W.-B.; Liu, T.; Yue, K.; Cheng, S. Z. D. *ACS Nano* **2016**, *10*, 6585−6596.

(4) Nam, K. T.; Shelby, S. A.; Choi, P. H.; Marciel, A. B.; Chen, R.; Tan, L.; Chu, T. K.; Mesch, R. A.; Lee, B.-C.; Connolly, M. D.; Kisielowski, C.; Zuckermann, R. N. *Nat. Mater.* **2010**, *9*, 454−460.

(5) Suzuki, Y.; Cardone, G.; Restrepo, D.; Zavattieri, P. D.; Baker, T. S.; Tezcan, F. A. *Nature* **2016**, *533*, 369−373.

(6) (a) Gonen, S.; DiMaio, F.; Gonen, T.; Baker, D. *Science* **2015**, *348*, 1365−1368. (b) Lotz, B. *Macromolecules* **2012**, *45*, 2175−2189.

(7) Qiu, H.; Gao, Y.; Boott, C. E.; Gould, O. E. C.; Harniman, R. L.; Miles, M. J.; Webb, S. E. D.; Winnik, M. A.; Manners, I. *Science* **2016**, *352*, 697−701.

(8) (a) Li, Z.; Chen, Z.; Cui, H.; Hales, K.; Qi, K.; Wooley, K. L.; Pochan, D. J. *Langmuir* **2005**, *21*, 7533−7539. (b) Li, Z.; Chen, Z.; Cui, H.; Hales, K.; Wooley, K. L.; Pochan, D. J. *Langmuir* **2007**, *23*, 4689−4694. (c) Li, Z.; Kesselman, E.; Talmon, Y.; Hillmyer, M. A.; Lodge, T. P. *Science* **2004**, *306*, 98−101. (d) Cui, H.; Chen, Z.; Zhong, S.; Wooley, K. L.; Pochan, D. J. *Science* **2007**, *317*, 647−650.

(9) Shimoni, E.; Rav-Hon, O.; Ohad, I.; Brumfeld, V.; Reich, Z. *Plant Cell* **2005**, *17*, 2580−2586.

(10) Austin, J. R.; Staehelin, L. A. *Plant Physiol.* **2011**, *155*, 1601−1611.

(11) Mustárdy, L.; Buttle, K.; Steinbach, G.; Garab, G. *Plant Cell* **2008**, *20*, 2552−2557.

(12) Seredyuk, V.; Alami, E.; Nydén, M.; Holmberg, K.; Peresypkin, A. V.; Menger, F. M. *Langmuir* **2001**, *17*, 5160−5165.

(13) (a) Zhang, W.-B.; Yu, X.; Wang, C.-L.; Sun, H.-J.; Hsieh, I.-F.; Li, Y.; Dong, X.-H.; Yue, K.; Van Horn, R.; Cheng, S. Z. D. *Macromolecules* **2014**, *47*, 1221−1239. (b) Yu, X.; Zhong, S.; Li, X.; Tu, Y.; Yang, S.; Van Horn, R. M.; Ni, C.; Pochan, D. J.; Quirk, R. P.; Wesdemiotis, C.; Zhang, W.-B.; Cheng, S. Z. D. *J. Am. Chem. Soc.* **2010**, *132*, 16741−16744. (c) Huang, M.; Hsu, C.-H.; Wang, J.; Mei, S.; Dong, X.-H; Li, Y.; Li, M.; Liu, H.; Zhang, W.; Aida, T.; Zhang, W.-B.; Yue, K.; Cheng, S. Z. D. *Science* **2015**, *348*, 424−428. (d) Yue, K.; Huang, M.; Marson, R. L.; He, J.; Huang, J.; Zhou, Z.; Wang, J.; Liu, C.; Yan, X.; Wu, K.; Guo, Z.; Liu, H.; Zhang, W.; Ni, P.; Wesdemiotis, C.; Zhang, W.-B.; Glotzer, S. C.; Cheng, S. Z. D. *Proc. Natl. Acad. Sci. U. S. A.* **2016**, *113*, 14195−14200.

(14) (a) Richardson, C. F.; Schuster, D. I.; Wilson, S. R. *Org. Lett.* **2000**, *2*, 1011−1014. (b) Sigwalt, D.; Holler, M.; Iehl, J.; Nierengarten, J.-F.; Nothisen, M.; Morin, E.; Remy, J.-S. *Chem. Commun.* **2011**, *47*, 4640−4642.

(15) (a) Burghardt, S.; Hirsch, A.; Schade, B.; Ludwig, K.; Böttcher, C. *Angew. Chem., Int. Ed.* **2005**, *44*, 2976−2979. (b) Yu, X.; Zhang, W.-B.; Yue, K.; Li, X.; Liu, H.; Xin, Y.; Wang, C.-L.; Wesdemiotis, C.; Cheng, S. Z. D. *J. Am. Chem. Soc.* **2012**, *134*, 7780−7787.

(16) Yin, P.; Lin, Z.; Wu, J.; Hsu, C.-H.; Chen, X.; Zhou, J.; Lu, P.; Eghtesadi, S. A.; Yu, X.; Cheng, S. Z. D.; Liu, T. *Macromolecules* **2015**, *48*, 725−731.

(17) Ma, S.; Hu, Y.; Wang, R. *Macromolecules* **2015**, *48*, 3112−3120.

(18) Yu, X.; Yue, K.; Hsieh, I.-F.; Li, Y.; Dong, X.-H.; Liu, C.; Xin, Y.; Wang, H.-F.; Shi, A.-C.; Newkome, G. R.; Ho, R.-M.; Chen, E.-Q.; Zhang, W.-B.; Cheng, S. Z. D. *Proc. Natl. Acad. Sci. U. S. A.* **2013**, *110*, 10078−10083.

(19) (a) Higuchi, T.; Tajima, A.; Motoyoshi, K.; Yabu, H.; Shimomura, M. *Angew. Chem., Int. Ed.* **2009**, *48*, 5125−5128. (b) Klinger, D.; Wang, C. X.; Connal, L. A.; Audus, D. J.; Jang, S. G.; Kraemer, S.; Killops, K. L.; Fredrickson, G. H.; Kramer, E. J.; Hawker, C. J. *Angew. Chem., Int. Ed.* **2014**, *53*, 7018−7022. (c) Jeon, S.-J.; Yi, G.-R.; Yang, S.-M. *Adv. Mater.* **2008**, *20*, 4103−4108.

(20) Chen, W. Y.; Zheng, J. X.; Cheng, S. Z. D.; Li, C. Y.; Huang, P.; Zhu, L.; Xiong, H.; Ge, Q.; Guo, Y.; Quirk, R. P.; Lotz, B.; Deng, L.; Wu, C.; Thomas, E. L. *Phys. Rev. Lett.* **2004**, *93*, 028301.

(21) Zheng, J. X.; Xiong, H.; Chen, W. Y.; Lee, K.; Van Horn, R. M.; Quirk, R. P.; Lotz, B.; Thomas, E. L.; Shi, A.-C.; Cheng, S. Z. D. *Macromolecules* **2006**, *39*, 641−650.

(22) Lin, Z.; Lu, P.; Hsu, C.-H.; Sun, J.; Zhou, Y.; Huang, M.; Yue, K.; Ni, B.; Dong, X.-H.; Li, X.; Zhang, W.-B.; Yu, X.; Cheng, S. Z. D. *Macromolecules* **2015**, *48*, 5496−5503.

(23) If adding NaOH aqueous solution (pH ≥ 9), the precipitation of giant surfactants is observed.

DOI: 10.1021/jacs.7b01275
J. Am. Chem. Soc. 2017, 139, 5883−5889